MMT adaptive secondary: first AO closed loop results

G. Brusa[a,b] A. Riccardi[b], F. P. Wildi[a],
M. Lloyd-Hart[a], H. M. Martin[a], R. Allen[a],
D. Fisher[a], D. L. Miller[a],
R. Biasi[c], D. Gallieni[d], F. Zocchi[e]

[a] Steward Observatory/Univ. of Arizona, 933 Cherry Av., Tucson AZ, 85721, USA
[b] INAF-Osservatorio Astrofisico di Arcetri, L.go E. Fermi 5, 50125 Firenze, Italy
[c] Microgate S.r.l, Via Stradivari 4, 39100 Bolzano, Italy
[d] ADS International S.r.L., Via Roma 87, 23868 Valmadrera (LC), Italy
[e] Media Lario S.r.l, Localitá Pascolo, 23842 Bosisio Parini (LC), Italy

ABSTRACT

The adaptive secondary for the MMT is the first mirror of its kind. It was designed to allow the application of wavefront corrections (including tip-tilt) directly at the secondary mirror location. Among the advantages of such a choice for adaptive optics operation are higher throughput, lower emissivity, and simpler optical setup. Furthermore, this specific implementation provides capabilities that are not found in most correctors including internal position feedback, large stroke (to allow chopping) and provision for absolute position calibration. The mirror has now been used at the MMT during several runs where it has performed reliably. In this paper we discuss the mirror operation and AO performance achieved during these runs in which the adaptive secondary has been operating in conjunction with a Shack-Hartmann wavefront sensor as part of the MMT adaptive optics system. In particular we mention a residual mirror position error due to wind buffeting and other errors of $\simeq 15$ nm rms surface and a stable closed loop operation with a 0dB point of the error transfer function in the range $20-30$ Hz limited mainly by the wavefront sensor maximum frame rate. Because of the location of the adaptive secondary with respect to the wavefront sensor camera, reimaging optics are required in order to perform the optical interaction matrix measurements needed to run the AO loop. This optical setup has been used in the lab but not replicated at the telescope so far. We will discuss the effects of the lack of such an internal calibration on the AO loop performances and a possible alternative to the lab calibration technique that uses directly light from sky objects.

Keywords: adaptive optics, deformable mirrors, adaptive secondary mirrors, electromagnetic actuators, capacitive sensors

1. INTRODUCTION

The first adaptive secondary (AS) to be used on the sky has had a relatively long development history that started with a seminal paper[1] presented ten years ago. We point to Ref. 2 and to the references therein for the details of the development. For a description of the unit and a discussion of the electro-mechanical aspects readers should refer to Ref. 3 and for the optical quality and more recent developments (like chopping) to Ref. 2. For what concerns the general performances achieved with the Multiple Mirror Telescope (MMT) adaptive optics that employs this AS we point to Ref. 4 (also presented at this conference). More details on the practical problems encountered and future work to make the AS operation a routine work are reported in Ref. 5 (also in this conference).

Here we will be concerned with some aspects of the operation of the adaptive optics (AO) system that are peculiar to the use of the adaptive secondary as well as some initial quantification of performance.

Further author information: (Send correspondence to G.B.)
G.B.: E-mail: gbrusa@as.arizona.edu, Telephone: ++1 520 626 9529

Astronomical Adaptive Optics Systems and Applications, edited by Robert K. Tyson, Michael Lloyd-Hart, Proceedings of SPIE Vol. 5169 (SPIE, Bellingham, WA, 2003)
0277-786X/03/$15 · doi: 10.1117/12.508411

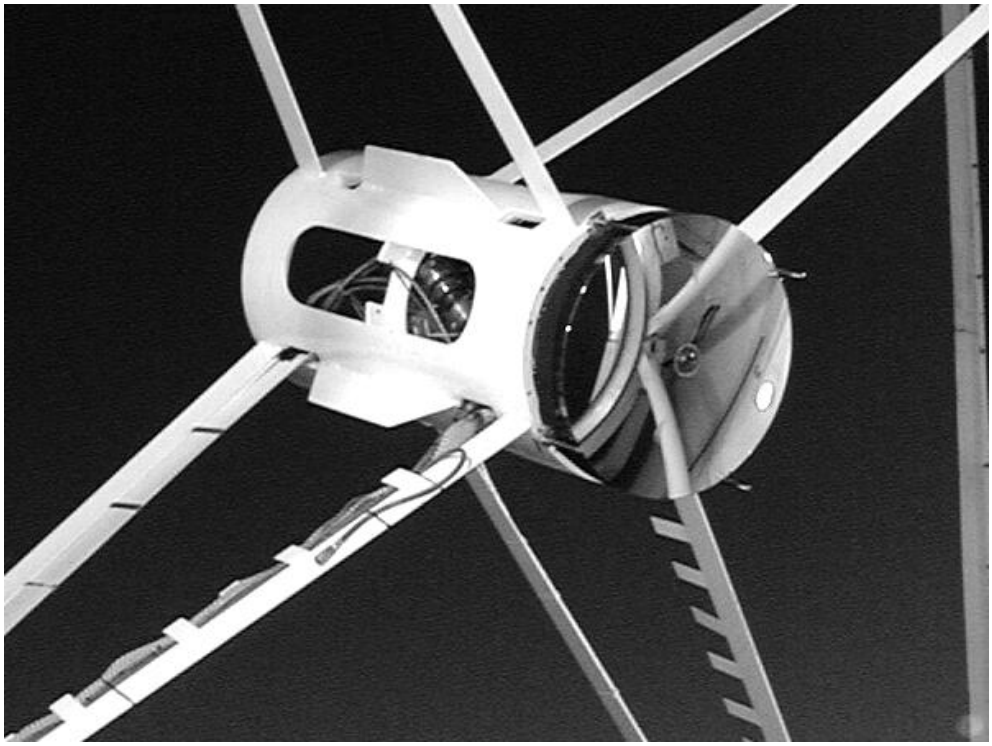

Figure 1. The adaptive secondary on the telescope. The photo was taken Jan 20, 2003 just before sunset at the MMT.

After the initial run (which we will call run 0) in June 2002 during which our system was affected by several hardware failures[2,6] much time was spent to partially refurbish the unit in order to fix two main problems encountered: the leak in cooling circuit and the fact that the unit was found to be 21 mm too long (given the magnitude, this error could not be compensated using the hexapod). After the repair three more observational runs (called run 1, 2, 3) have been carried out, in November 2002, January and May 2003 respectively, at the MMT. These runs have been successfull producing two science papers (see Ref. 7, 8).

During the observational runs 1, 2 and 3 the adaptive optics system used a reconstructor based on lab derived interaction matrix data (Feb 2002). Initially this was a concern since we were not sure how well the telescope optical alignment between wavefront sensor and adaptive secondary reproduced that used in the lab. Our experience at the telescope has shown that this is not a serious problem (see Ref. 4 for details on Strehl achieved in various conditions). Nevertheless the exact quantification of the limitations in the performances due to this aspect of our AO system is yet to be fully determined. In particular it would be interesting to determine what is the actual limit of this reconstructor and how many mirror modes (these are the feed-forward modes, see Ref. 3) can be used reliably before the correction becomes ineffective or, worse, degrades the overall performance. One direct way to quantify this error is to compare the performances obtained at the science camera level (in terms of Strehl) with what is expected from the residual error seen on WFS for very bright reference objects. This assumes that other errors like non-common path aberrations are negligeable, but this analysis can nevertheless set an upper limit to the total effect of the reconstructor error. This matter is discussed in Sec. 2 and a specific case of good seeing is presented there.

In Sec. 3 we discuss a technique that could be used to refine our knowledge of the reconstructor for the AO loop operation. This is based on measurements taken during closed loop operation on the sky and assumes we are able to apply a time modulated slope offset signal.

2. AO CLOSED LOOP PERFORMANCES

In this section we will attempt a first quantification of the performances achieved by the adaptive optics (AO) loop. This is done by analyzing data saved by the wavefront computer (WFC) during the AO operation. From these data it is possible to compute the rms residual wavefront error as seen from the wavefront sensor (WFS) and to estimate the input rms wavefront error that the loop is trying to correct. From the input wavefront error it is possible to estimate the level of seeing and therefore the rms wavefront error not seen by the WFS (this is essentially the fitting error). From this total residual wavefront error one can compute the expected Strehl at the observing wavelength and compare this with the actual observed Strehl in the science camera focal plane. In general the observed Strehl will be lower than the expected one and this is a measure of both our non-common path wavefront errors (static errors) and the ability of the reconstructor used in the AO operation to properly reconstruct the wavefront error. Both these terms can be thought of as calibration errors.

2.1. Notation

In Fig.2 we show a diagram of the AO loop and introduce the notation used for the rest of the paper. The main physical elements are: the WFS (a 12x12 sub-aperture Shack-Hartmann), the adaptive secondary, the slope calculator (SSC) and the real-time reconstructor (RTR). G is the applied loop gain while G' is a gain factor that depends on the seeing conditions and on the quality of the correction. The other components describe the time filtering used on the loop (an integrator) and the transition from continuous system (S) to discrete and back to continuous (H). The symbols without boxes represent the signals that the WFC can store in its internal memory as a time history. The WFC can save the time history of camera frames (f), computed slopes (s), reconstructed mirror commands (r), mirror commands (c) , mirror position (p) and other parameters such as mirror currents. Finally, $\tilde{t}$ and $\tilde{e}$ represent the input turbulence and the residual error and we will use t and e to represent the same signals projected in the space spanned by the reconstructor modes.

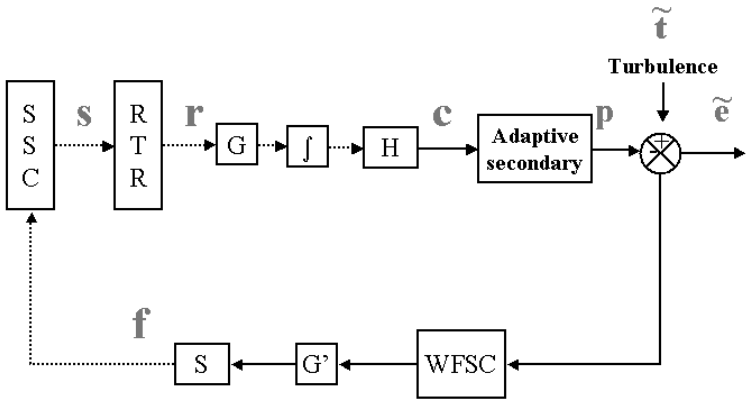

Figure 2. AO loop diagram showing the main components and signals (see text).

2.2. System analysis

The system analysis can be performed in both the time domain and the frequency domain. In order to simplify the analysis we decided to work in the time domain and to approximate the time response of the loop as a time delay plus the integrator (see also Sec. 3) so that for the reconstructed modes we can write $c(t_i) = c(t_i - t_{delay}) + G\,G'\,e(t_i - t_{int} - t_{delay})$ where the operations performed by the WFS and by the reconstructor

have been omitted (since they cancel out) in the last term. Here t_i is a discrete time variable, t_{int} is the integration time of the camera and t_{delay} is the frame conversion time of the camera. In fact, t_i and t_{int} are both integer multiples of t_{delay} ($\simeq 1.8$ ms). To simplify the analysis we assume that the adaptive secondary settling time is negligeable; in fact it is on the order 1 ms and it depends on the specific spatial mode considered (see Ref. 3). This assumption causes a small error affecting the loop behavior at high frequencies where the turbulent signal is extremely small. This approximation would be poor if considering the compensation of the tip-tilt induced by the telescope vibrations that are in the range 20-40 Hz, in which case the effect of the adaptive secondary temporal response should be taken into account. In the following we will analyze the performance of the loop for all the higher order modes excluding the tip-tilt term. This is because this term is dominated by telescope vibrations that cannot be properly compensated by the AO loop and will have to be dealt with by other means, by either eliminating the source of vibrations or, for instance, by using a feedforward signal that drives directly the mirror correction bypassing the AO loop. Another paper[4] also presented at this conference discuss more extensively the tip-tilt term.

The spatial sampling of the WFS limits the spatial order up to which the analysis can be performed, so that a fitting error term must be added to obtain the total rms (this is the difference between e and $\tilde{e}$). Moreover since in this preliminary analysis we are only interested in quantifying the calibration error we have not introduced a WFS noise term. Once a residual wavefront error has been estimated we will compare the expected Strehl ratio from this model with the one measured with our engineering camera operating in H-band ($1.65\mu m$).

2.3. Data calibration

The mirror command and position can be converted directly to optical path difference (OPD) thanks to the internal capacitive position sensors *. The wavefront slopes instead are computed using the quad-cell response measured in the lab with a diffraction limited spot and, in order to obtain the actual value of the slopes on the sky, we need to introduce a factor that is a function of the level of turbulence and of the quality of the correction. This factor (called G') was not determined during the observations in closed loop and must be inferred by other observations. In our case we used frames taken at higher spatial resolution with the WFS camera to determine G'.

The camera of our WFS (a 12x12 SH)[9] can run in two different formats: a 72x72 mode in which for each sub-aperture a 6x6 pixel sub-frame is output, and a 24x24 mode for which 2x2 super-pixels (each of which is a 3x3 binning of the original array) sub-frame is output per sub-aperture. When the camera operates in unbinned mode the shortest read-out time is 9 ms and a 'slow' loop can be run, bypassing the real-time WFC and using instead a PC to perform closed loop operation. We can use the unbinned frames taken with the slow loop to determine the average Strehl ratio over a sub-aperture and from this value we can determine the reduction factor G' in our quad-cell response. The determination of the sub-aperture Strehl can be done by using those sub-apertures for which the spots by chance are 'well centered', say to within a 20% quad-cell unbalance, and comparing the average illumination of these sub-arrays obtained in the seeing limited spot with the one obtained with a diffraction limited spot. Of course this is quite an indirect method of determining the seeing and in the future we will make sure to have a direct measurement of the quad-cell response.

2.4. A specific case study

We focus our analysis to data taken January 19, 2003 during very good seeing conditions. During these observations we collected ten sets of full data (f,s,r,p,c) each consisting of 1000 time samples taken at 1.8ms (full speed). The AO loop was reconstructing 52 mirror modes with an average G of 0.3. Almost at the same time that these data were collected, full resolution loop data were taken that allow us to estimate the factor G'. As can be seen in Fig. 3 the central intensity of the spot in high resolution mode for the seeing limited case is $\simeq 60\%$ of the diffraction limited one. If we assume that the shape of the main core of the spot did not change significantly (i.e. it is still of the size of the diffraction limit), we derive an equivalent reduction of the Strehl ratio and of the quad-cell response (that is proportional to the Strehl ratio) or a factor $G' \simeq 0.6$. To properly scale the WFS data a factor $1/G' \simeq 1.7$ has to be applied.

*In fact the internal position sensors were never calibrated directly and we are using the nominal calibrations. This introduces a small error for the strokes used by the AO loop.

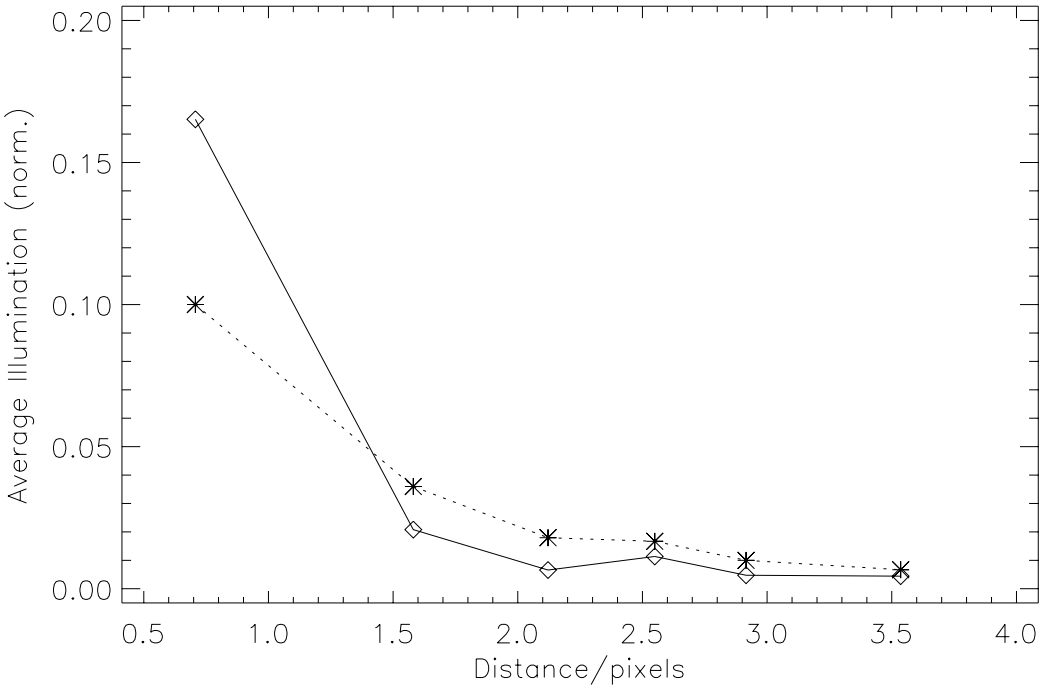

Figure 3. Average intensity seen by the WFS operating in unbinned mode for 'well centered' spots. Solid line: diffraction limited case, dashed line: seeing limited case.

To compute the total residual rms error ($\tilde{e}$) two similar methods can be used. One consists in using the reconstructed error (r) which will contain all the mirror modes up to order N (where N is the order of the reconstructor, or 52 in our case) and to add to this the residual error due to the turbulence not reconstructed. The second method (used here) consists in using a syntethic reconstructor, built using an interaction matrix between Zernike modes over the entrance pupil and SH sensor output, to compute the residual error up to a certain Zernike order and to add to this first term the residual error for all the remaining orders in quadrature. The maximum Zernike order has to be picked in such a way that it represents all the possible corrections applicable by the mirror when a reconstructor of order N (52 in our case) is used. Of course in order to add the correct amount of fitting error an estimate of the turbulence in terms of r_0 has to be determined. The determination of the turbulence strength can be done using the reconstructed signal t=p+e, by analyzing it in terms of Zernike modes and then fitting the result with the expected behavior for Kolmogorov turbulence.

In Fig. 4 we summarize the results obtained for the specific case considered. The residual error e decomposed in Zernike modes (up to the 8th order) is shown together with its uncalibrated value (G'=1), the turbulence signal t up to the same Zernike order is also shown. The fitting of the turbulence gives a value of $D/r_0 \simeq 25$ in V-band corresponding to a seeing of 0.35 arcsec in the H-band. The fitting was peformed excluding the lowest three Zernike orders in order not to be sensitive to effects of outer scale and possibly long time correlation of the low order modes. [†] One important feature to notice is the presence of power higher than average at the end of each order for orders above the 5th. These modes are much better represented with the reconstructor used (52 mirror modes) than the other belonging to the same order but are probably also more sensitive to optical mis-alignments.

If we consider the correct value for the factor G' (0.6) and the fit of the value of r_0 we can compute the values

[†]The latter can in fact be excluded in this case since the time correlation function for these modes shows a relatively 'fast' seeing.

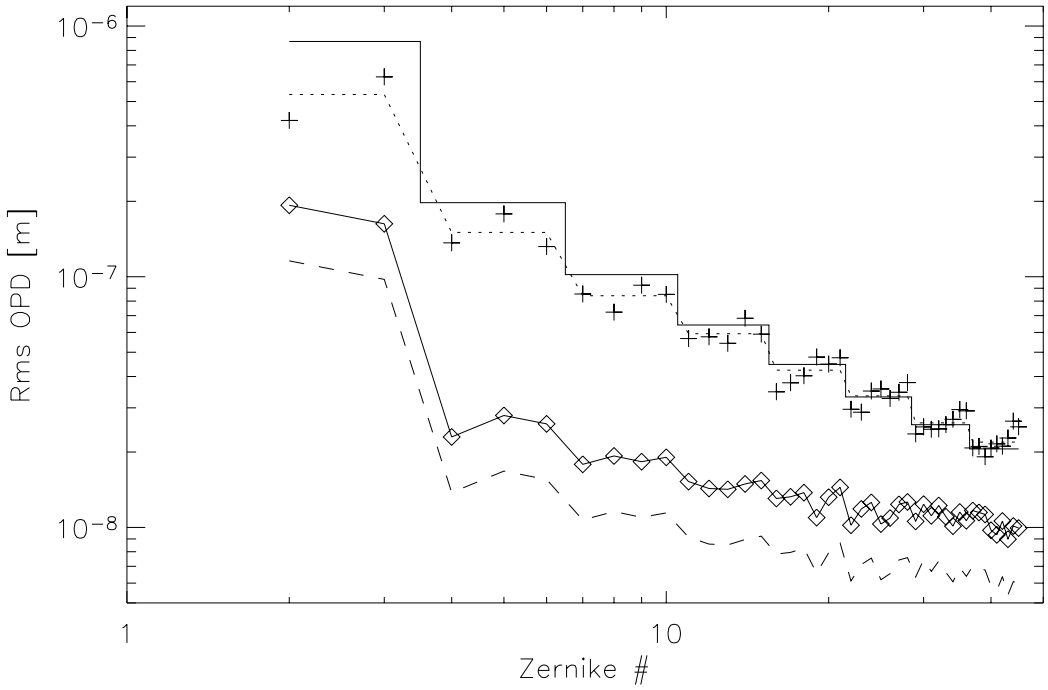

Figure 4. Average (over ten data sets) rms decomposed in Zernike modes for various signals. Solid line and diamonds: residual wavefront as seen from the WFS (dashed line un-calibrated data). Crosses: turbulent signal (dashed line average over each order). Solid line: fit with Kolmogorov turbulence ($D/r_0 \simeq 25$ in V-band).

	wfs rms error [nm]	
	G'=1.0	G'=0.6
modes 2,3	151 (14)	265 (25)
modes 4-45	55	97
modes 45-∞	128	128
mirror	80	80
total-ho	160	179

Table 1. Estimated rms wavefront error decomposed in its various contributions for uncalibrated data (G'=1) and calibrated one (G'=0.6). The turbulence contributions are from the same data shown in Fig.4 , the mirror term is from mirror flattening data (see Ref.2). The last row is the total rms wavefront error tip-tilt removed. The numbers in parentheses in the first line are the equivalent single axis tip-tilt jitter in mas.

for the rms errors reported in Tab.1. The total high order rms error (last row in Tab.1) is not very sensitive to the value of G' since this only affects the term of the corrected Zernike (modes 4-45).

2.5. PSF analysis

As we already mentioned a direct way to quantify the calibration error that includes both non-common path aberrations and reconstructor error is to compare the performances obtained at the science camera level (in terms of Strehl) with what is expected from the residual error seen on WFS for very bright reference objects. Since we do not have yet a way of determining the non-common path term, the results of the analysis cannot be directly translated into actual errors in the wavefront reconstruction. The analysis can nevertheless set an upper limit to the reconstructor error. We took simultaneous data with an engineering infrared camera in H-band with short integration time (1 ms). By shifting and adding about 300 frames taken of the guide star used by the loop

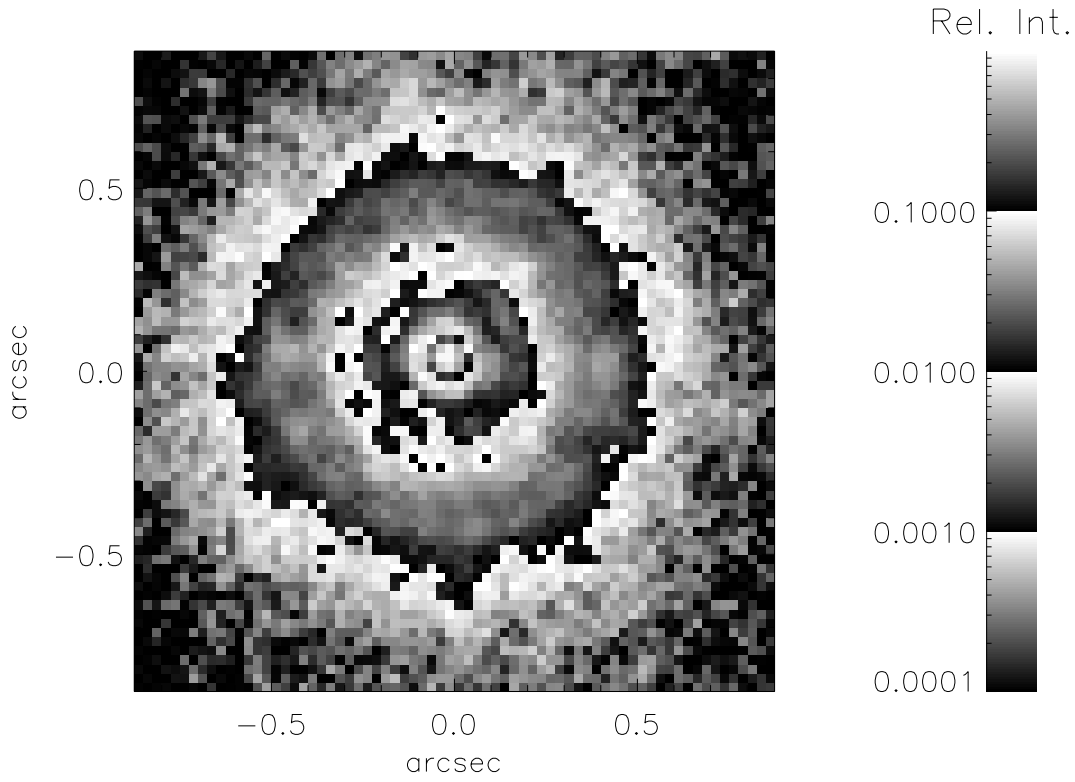

Figure 5. Average AO PSF tip-tilt removed (see text for details). The pixel scale is 25 mas/pixel. Four orders of magnitude are represented by a logarithmic look up table repeated four times. Most of the pattern is relatively smooth, except for the presence of a correlated pattern in the range between 10^{-2} and 10^{-3} whose presence is yet to be understood.

we built an average, tip-tilt removed, PSF shown in Fig.5. In Fig.6 a cross section is compared with a theoretical diffraction limited one. For this image we computed an achieved strehl of $\simeq 40\%$ vs. an expected strehl (from Tab.1) of over 60%. This sets a limit to the total calibration error (assuming that these errors are not correlated to the other ones) to $\simeq 170$ nm rms. This error is of the same magnitude of the loop residual error and so it is important to try to reduce it.

2.6. Mirror tracking errors

In this section we discuss the error between mirror commands and mirror positions for the case studied above. In Fig.7 the average rms of the mirror commands and commands minus position is shown as a function of the mirror mode. The total rms error is $\simeq 15$ nm in surface. There are several contributions to this error:

- wind buffeting;
- temporal tracking;
- internal mirror calibration.

The first contribution is certainly higher at lower mode number and was measured previously (see Ref. 2) to be on the order of 5-10 nm rms for the same ground wind speed (between 20 and 30 Km/h). The second contribution is mostly in the first two modes that are essentially tip-tilt; for these both the presence of telescope vibrations in the frequency range of 20-40 Hz and a slightly reduced bandwidth due to a longer mirror response time contribute to increasing the residual tracking error. The last item depends on errors in the mirror internal position calibration.

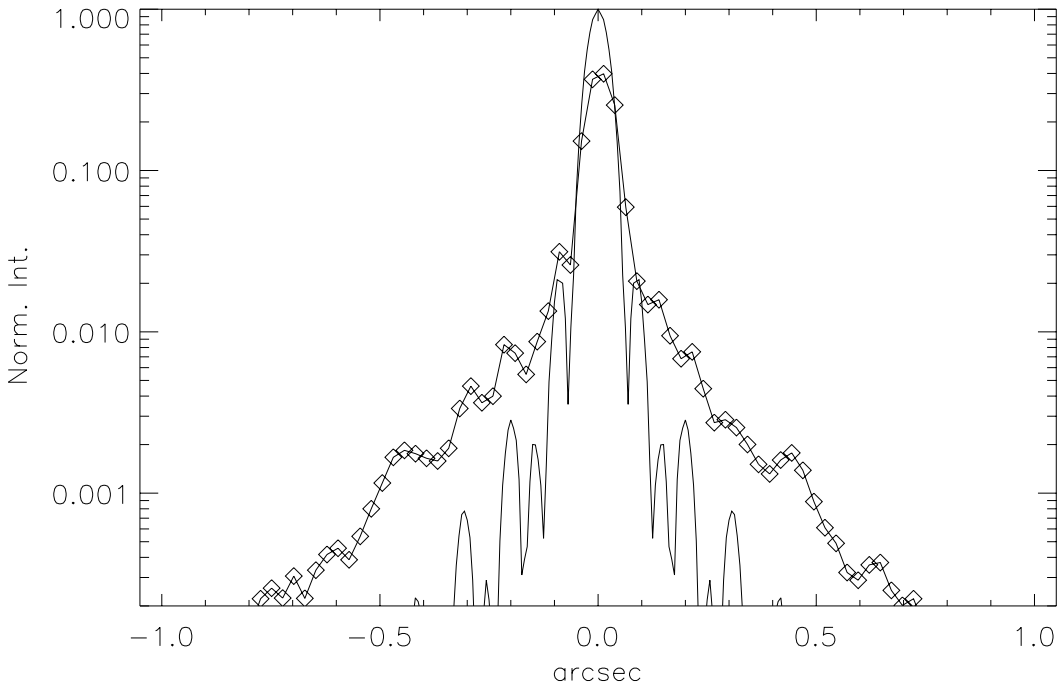

Figure 6. Cross section of the PSF shown in Fig.5 (solid line and diamonds) compared with a diffraction limited one (solid line). For this last the central obscuration has been taken into account.

It should be pointed out that this estimate is a lower bound since only a time history taken at the WFS sampling time could be used and therefore the contribution due to the mirror settling time is not included (see Ref. 3).

3. FUTURE DEVELOPMENTS

In this section we analyze in detail the frequency response of the loop and discuss a technique that we are planning to use in the near future to refine the reconstructors used so far. This new technique uses data taken on the sky with the AO loop running as currently we do not have any way of using the optical setup used in the lab. With this technique we hope to be able to produce a more accurate high order reconstructor and fix some of the suspected alignment problems mentioned in the introduction.

In Fig.8 the AO loop diagram of Fig. 2 is redrawn with emphasis on the frequency and spatial response of the main components: the sensing one (essentially the WFS) and the system one that includes both the loop time filtering and the adaptive secondary. The time response of the WFS (see Eq.2) is modeled as a running mean of time window T (integration time) plus a delay T (read-out time). This corresponds to the case in which the WFS is running at full speed integrating for a time T equal to the frame conversion time (1.8 ms in our case). The system (and filter) term are modeled as an integrator plus the effect of the hold at the output of the WFC (see Fig.2). The mirror transfer function will be considered 1 in this analysis. From Eq.2 it can be seen that the temporal response of the WFS when $\pi f T \ll 1$ can be approximated by a pure time delay as claimed in Sec.2 (the term $sinc(\pi\, f\, T) \simeq 1$) .

For what concerns the spatial representation of the turbulent signal we used the reconstructor mirror modes (assumed to be continuous functions over the system entrance pupil) plus a second (infinite) set of modes that toghether with the first set forms a complete representation for the wavefronts (see for instance Ref. 10). In this way the operation that converts wavefronts to slopes can be represented by the infinte matrix D while the

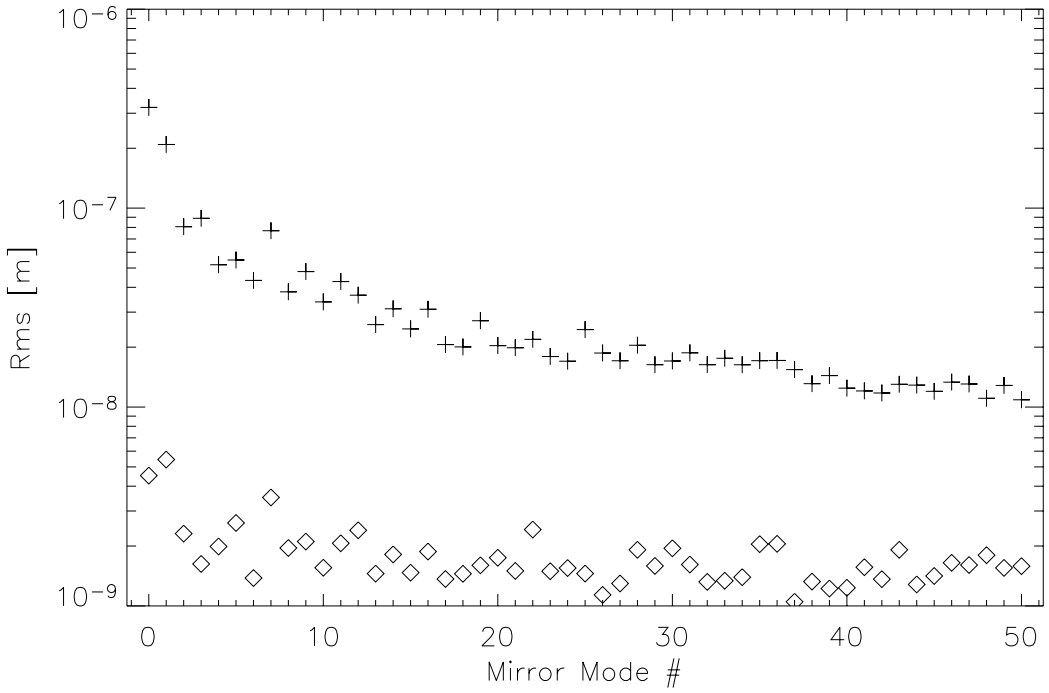

Figure 7. Plot of the rms mirror commands (crosses) and rms mirror position error (diamonds) decomposed in mirror modes.

operation of the reconstructor by the finite matrix $\overline{D}^{+}$. This last is the pseudo-inverse of the interaction matrix $\overline{D}$ measured in the lab .

We intend to use the possibility of introducing slope offsets (see Fig.8) to refine our knowledge of the reconstructor. We know that, in the case of a perfect reconstructor, if we apply a step to the slope offset (at point s_{off}) corresponding to a singular vector s_i of the reconstructor we will obtain that (after a time of the order of the time response of the loop) the loop applies to the mirror the corresponding singular vector p_i, this produces the same set of slopes (with a minus sign) and the slopes offset is exactly canceled.

In the case of an imperfect reconstructor two things will happen: the set of slopes will not cancel exactly (i.e. a residual s' with $\mid s' \mid > 0$ will be measured) and the mirror will be in general driven with a linear combination of the singular vectors $\Sigma \alpha_j \, p_j$ (in which the singular vector p_i will be dominant).

By measuring these residuals it is possible in principle to refine our knowledge of the reconstructor. In our case this measurement has to be done with a sky source illuminating our AO optics, therefore our measurement will be affected by the noise introduced in the loop by the atmospheric turbulence. Our plan is to reduce the effect of this noise by introducing a time modulation of the slope offset signal. In particular by using a sinusoidal modulation we can have a very precise knowledge of the relative phase between the various signals by using our model of the system. Simple algebra gives two main relationships (see Fig.8):

$$s \, = \, -h_{sens} \, D \, p \quad , \quad (1 + h_{ol} \, D \, \overline{D}^{+}) \, s \, = \, -h_{ol} \, D \, \overline{D}^{+} \, s_{off} \tag{1}$$

where

$$h_{sys} \, = \, G \, h_{int} \, h_{hold} \, = \, G \, \frac{1}{2i\pi f} \, e^{-i\pi T f} \quad , \; h_{sens} \, = \, G' \, h_{wfs} \, = \, G' \, sinc(\pi \, f \, T) \, e^{-3i\pi T f} \tag{2}$$

and $h_{ol} \, = \, h_{sys} \, h_{sens}$. The first term in Eq.1 gives the general relation between mirror position and slope signal while the second shows what slopes s can be introduced by using the input s_{off}, setting a limit in both

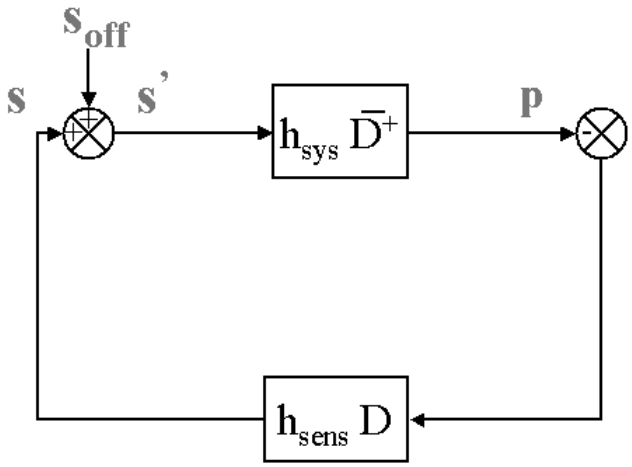

Figure 8. Diagram of the AO loop showing where the slope offsets are injected and the various signals used to improve the estimate of the reconstructor. See Eq.2 for a definition of the symbols used.

temporal frequency and spatial domain. By applying the entire set of singular vectors s_k with k=1-N to s_{off} and measuring the corresponding values for p a fit of the matrix D (restricted to the space spanned by the singular vectors p_k) can be performed. Concerning the frequency to be used for the temporal modulation it is obvious from Eq.1(right) that it should be lower than the closed loop control bandwidth of the system ($\simeq$ 30 Hz), in order to introduce a significant modulation amplitude. On the other hand this frequency should be high enough to take advantage of the roll-off of the signal generated by the AO correction of the turbulence.

4. CONCLUSIONS

After an initial difficult telescope run where we had to face several mechanical failures of the adaptive secondary for the MMT telescope[2,6] we have had three very successful runs during which we were able to collect both very valuable engineering data and science data. At this moment the adaptive secondary seems to be well characterized from the electro-mechanical and optical point of view. Moreover, during the telescope runs, practical information about the operation of this device at the telescope has been collected. We are entering a new phase where more detailed analysis is needed on the behavior of the AO loop itself. This paper is a first attempt to give such an analysis and it shows that some calibration errors may be limiting the AO performance. Given the current lack of appropriate optical setup for measurement of the AO interaction matrix, we intend to explore a new technique to refine our reconstructor using data collected during AO closed loop operation.

ACKNOWLEDGMENTS

We would like to thank Laird Close for the H-band data used for the PSF analysis. We would also like to thank Richard Gonzalez-Sosa, Manny Montoya, Matt Rademacher, Mario Rascon and Dylan Curley for their essential contribution to the work in the lab and at the telescope. We are very thankful to the MMT crew for their patience and very valuable help. This work has been supported by the Air Force Office of Scientific Research under grant AFOSR#F49620-01-1-0383.

REFERENCES

1. P. Salinari, C. Del Vecchio, and V. Biliotti, "A study of an adaptive secondary mirror," in *ICO 16 Satellite Conference on Active and Adaptive Optics*, F. Merkle, ed., *ESO Proc.* **48**, pp. 247–253, 1993.
2. G. Brusa, A. Riccardi, P. Salinari, F. P. Wildi, M. Lloyd-Hart, H. M. Martin, R. Allen, D. Fisher, D. L. Miller, R. Biasi, D. Gallieni, and F. Zocchi, "MMT adaptive secondary: performance evaluation and field testing," in *Adaptive Optical System Technologies II. Edited by Wizinowich, Peter L.; Bonaccini, Domenico. Proceedings of the SPIE, Volume 4839, pp. 691-702 (2003).*, pp. 691–702, February 2003.
3. A. Riccardi, G. Brusa, C. del Vecchio, P. Salinari, R. Biasi, M. Andrighettoni, D. Gallieni, F. Zocchi, M. Lloyd-Hart, F. Wildi, and H. M. Martin, "The adaptive secondary mirror for the 6.5 conversion of the Multiple Mirror Telescope," in *Beyond Conventional Adaptive Optics*, 2001.
4. F. P. Wildi, G. Brusa, M. Lloyd-Hart, L. Close, and A. Riccardi, "First light of the 6.5-m MMT adaptive optics system," in *In these proceedings*,
5. M. Lloyd-Hart, G. Brusa, F. P. Wildi, and A. Riccardi, "Lessons learned from the first adaptive secondary mirror," in *In these proceedings*,
6. F. P. Wildi, G. Brusa, A. Riccardi, M. Lloyd-Hart, H. M. Martin, and L. M. Close, "Towards 1st light of the 6.5m MMT adaptive optics system with deformable secondary mirror," in *Adaptive Optical System Technologies II. Edited by Wizinowich, Peter L.; Bonaccini, Domenico. Proceedings of the SPIE, Volume 4839, pp. 155-163 (2003).*, pp. 155–163, February 2003.
7. L. M. Close, F. P. Wildi, M. Lloyd-Hart, G. Brusa, D. Fisher, D. L. Miller, A. Riccardi, P. Salinari, D. W. McCarthy Jr., R. Angel, R. Allen, H. M. Martin, R. G. Sosa, M. Montoya, M. Rademacher, M. Rascon, D. Curley, N. Siegler, and W. J. Duschl, "High Resolution Images of the Trapezium Cluster: First Scientific Results from the MMT Deformable Secondary Mirror Adaptive Optics System," *Submitted to The Astrophysical Journal* .
8. L. M. Close, B. Biller, W. Hoffmann, P. Hinz, J. Bieging, F. P. Wildi, M. Lloyd-Hart, G. Brusa, D. Fisher, D. L. Miller, and R. Angel, "Mid-Infrared Imaging of the Post-AGB Star AC Herculis with the MMT Adaptive Optics System ," *Submitted to The Astrophysical Journal (letters)* .
9. T. A. Rhoadarmer, P. C. Mcguire, J. M. Hughes, M. Lloyd-Hart, J. R. P. Angel, S. Schaller, and M. A. Kenworthy, "Laboratory adaptive optics system for testing the wavefront sensor for the new MMT," in *Proc. SPIE Vol. 3762, p. 161-173, Adaptive Optics Systems and Technology, Robert K. Tyson; Robert Q. Fugate; Eds.*, pp. 161–173, September 1999.
10. E. Gendron and P. Lena, "Astronomical adaptive optics. 1: Modal control optimization," *Astronomy and Astrophysics* **291**, pp. 337–347, November 1994.